Subantarctic mode water in the southeast Pacific: Effect of exchange across the Subantarctic Front

J. W. Holte,[1] L. D. Talley,[2] T. K. Chereskin,[2] and B. M. Sloyan[3]

Received 3 August 2012; revised 24 January 2013; accepted 23 February 2013; published 23 April 2013.

[1] This study considered cross-frontal exchange as a possible mechanism for the observed along-front freshening and cooling between the 27.0 and 27.3 kg m^{-3} isopycnals north of the Subantarctic Front (SAF) in the southeast Pacific Ocean. This isopycnal range, which includes the densest Subantarctic Mode Water (SAMW) formed in this region, is mostly below the mixed layer, and so experiences little direct air-sea forcing. Data from two cruises in the southeast Pacific were examined for evidence of cross-frontal exchange; numerous eddies and intrusions containing Polar Frontal Zone (PFZ) water were observed north of the SAF, as well as a fresh surface layer during the summer cruise that was likely due to Ekman transport. These features penetrated north of the SAF, even though the potential vorticity structure of the SAF should have acted as a barrier to exchange. An optimum multiparameter (OMP) analysis incorporating a range of observed properties was used to estimate the cumulative cross-frontal exchange. The OMP analysis revealed an along-front increase in PFZ water fractional content in the region north of the SAF between the 27.1 and 27.3 kg m^{-3} isopycnals; the increase was approximately 0.13 for every 15° of longitude. Between the 27.0 and 27.1 kg m^{-3} isopycnals, the increase was approximately 0.15 for every 15° of longitude. A simple bulk calculation revealed that this magnitude of cross-frontal exchange could have caused the downstream evolution of SAMW temperature and salinity properties observed by Argo profiling floats.

Citation: Holte, J. W., L. D. Talley, T. K. Chereskin, and B. M. Sloyan (2013), Subantarctic mode water in the southeast Pacific: Effect of exchange across the Subantarctic Front, *J. Geophys. Res. Oceans*, *118*, 2052–2066, doi:10.1002/jgrc.20144.

1. Introduction

[2] Strong westerly winds over the Southern Ocean propel the Antarctic Circumpolar Current (ACC). During winter, deep mixed layers form north of the Subantarctic Front (SAF), the northernmost front of the ACC. *McCartney* [1977] named these deep winter mixed layers Subantarctic Mode Water (SAMW). SAMW becomes progressively colder, fresher, and denser as it nears Drake Passage from the west [*McCartney*, 1977; *England et al.*, 1993; *Talley*, 1996; *Hanawa and Talley*, 2001]. SAMW is characterized by low potential vorticity (PV) and high oxygen content and is important to many global-scale processes. It forms part of the upper limb of the global overturning circulation [*Sloyan and Rintoul*, 2001], renewing the lower thermocline in the southern hemisphere's subtropical gyres [*McCartney*, 1982]. The heat, freshwater, and carbon transports associated with SAMW's global-scale circulation make it relevant to the Earth's climate and to the ocean's global overturning circulation [*Keeling and Stephens*, 2001; *Pahnke and Zahn*, 2005].

[3] Many processes contribute to the formation of the deep winter SAMW mixed layers, including air-sea fluxes, wind-driven mixing, and cross-frontal exchange. Studies have shown that turbulent mixing driven by buoyancy loss and wind forcing is essential for forming the deep SAMW mixed layers [*Wang and Matear*, 2001; *Sloyan et al.*, 2010; *Holte et al.*, 2012]. *McCartney* [1977] credited the cumulative effects of air-sea fluxes of heat and precipitation with driving the observed eastward freshening and cooling of SAMW from south of Africa to Drake Passage. Recent studies have demonstrated that the interannual variability of SAMW is primarily driven by variations in buoyancy fluxes [*Naveira-Garabato et al.*, 2009; *Vivier et al.*, 2010]. Other studies, however, have found that Ekman transport dominates the temporal variability of SAMW properties and that air-sea fluxes cannot account for the observed temporal variability of SAMW [*Speer et al.*, 2000; *Sloyan and Rintoul*, 2001; *Rintoul and England*, 2002].

[4] Cross-frontal exchange, in the form of ACC meanders and eddies, Ekman transport, and intrusions, can penetrate the strong PV gradient associated with the SAF and contribute to the downstream evolution of SAMW by

[1]Woods Hole Oceanographic Institution, Woods Hole, Massachusetts, USA.
[2]Scripps Institution of Oceanography, University of California, San Diego, California, USA.
[3]Center for Australian Weather and Climate Research, CSIRO Marine and Atmospheric Research, Hobart, Tasmania, Australia.

Corresponding author: J. W. Holte, Woods Hole Oceanographic Institution, 86 Water St, Woods Hole, MA 02543, USA. (jholte@whoi.edu)

2169-9275/13/10.1002/jgrc.20144

transporting cold, fresh waters from the Polar Frontal Zone (PFZ) across the ACC. Eddies, identified as distinct cold or warm core rings or as deviations from a long-term mean, have been shown to transport polar waters across the ACC and to disperse those waters via mechanical mixing. *Ansorge et al.* [2006] found that eddies were likely to be significant in maintaining local heat budgets in the SAMW formation region north of the SAF; they also argued that the meridional heat and salt fluxes associated with the eddies must be adequately quantified for incorporation into climate models. *Sokolov and Rintoul* [2009b] found that eddy-induced exchange across the SAF was particularly strong in the southeast Pacific. Eddies have been shown to modify Ekman transport and air-sea fluxes [*Sallée et al.*, 2008] and to influence SAMW property variability [*Herraiz-Borreguero and Rintoul*, 2010]. *Morrow et al.* [2004] observed that cyclonic eddies southwest of Tasmania penetrated to 1500 m depth and carried cold, fresh water into the SAMW formation region. *Jayne and Marotzke* [2002] have shown that the majority of eddy heat transport across the ACC was in the upper 1000 m. Studies investigating the relationship between ACC eddy diffusivities and PV gradients [*Marshall et al.*, 2006; *Abernathey et al.*, 2010] and the mean flow [*Shuckburgh et al.*, 2009; *Ferrari and Nikurashin*, 2010] have shown that lower cross-stream PV gradients and lower mean flows generally correspond to higher eddy diffusivities.

[5] Many studies have looked at the importance of cross-frontal intrusions, including Ekman transport, to the SAMW and Antarctic Intermediate Water (AAIW) layers. Intrusions are generally viewed as evidence for strong lateral fluxes of heat and salt and indicate subsurface lateral exchange between water masses [*Joyce*, 1977; *Ruddick*, 2003]. *Dong et al.* [2008] found that Ekman transport could contribute to SAMW formation in the Indian Ocean. *Ito et al.* [2010] identified Ekman transport as the primary mechanism for the transport of anthropogenic CO_2 across the ACC. Northward Ekman transport is approximately balanced by southward eddy transport [*Karsten and Marshall*, 2002; *Sallée et al.*, 2010]. *Park and Gambéroni* [1997], in the Indian Ocean, found that cross-frontal injections of AAIW across the SAF were not continuous in time and space but occurred impulsively and were associated with meanders and eddies in the ACC.

[6] In this study, we used observations from two recent hydrographic cruises and an optimum multiparameter (OMP) analysis [*Tomczak and Large*, 1989] to estimate the cumulative exchange, via transport and mixing, across the SAF in the southeast Pacific Ocean and its effect on SAMW properties. The first cruise, in austral winter (23 August to 5 October 2005), observed the deep SAMW mixed layers; the second cruise occupied the same cruise track in austral summer (30 January to 14 March 2006) and observed the subsequent restratification of the SAMW. Each cruise crossed the SAF at multiple longitudes, providing two approximately synoptic data sets useful for examining along- and cross-frontal property distributions and the along-front evolution of SAMW. Numerous instances of cross-frontal exchange were observed during both cruises: intrusions crossing the SAF were evident in the conductivity-temperature-depth (CTD)/Rosette/Lowered Acoustic Doppler Current Profiler (LADCP) data, cold-core eddies were observed in the SAMW formation region during the winter cruise, and a fresh surface layer capped the SAMW during the summer cruise, perhaps due to Ekman transport across the SAF. The temperature, salinity, oxygen, and nutrient data sets from both cruises were incorporated into an OMP analysis to estimate the overall cross-frontal exchange along various subsurface isopycnal ranges denser than SAMW. OMP analysis, an inverse method typically used to examine the spreading and mixing of water masses, was useful for tracking the exchange of waters from the PFZ with the SAMW formation region; in our analysis, it provided an estimate of the cumulative exchange accomplished by a combination of Ekman transport, eddies, and intrusions. In a companion study, *Holte et al.* [2012] demonstrated that, on seasonal time scales, air-sea fluxes and wind-driven mixing were strong enough to deepen the SAMW mixed layers in the southeast Pacific but did little to alter the SAMW temperature and salinity properties. A simple bulk calculation using the OMP results revealed that cross-frontal exchange could account for much of the downstream evolution of SAMW properties observed by Argo.

[7] The remainder of the manuscript is organized as follows: section 2 describes the cruise and other data used in the analysis, section 3 describes the observations of cross-frontal exchange, and section 4 outlines the OMP method and its results. Section 5 summarizes the findings and considers the implications of the cross-frontal exchange for SAMW formation.

2. Data

[8] Two hydrographic surveys conducted on R/V Knorr in the southeast Pacific Ocean collected high quality, synoptic observations of the SAF and the SAMW formation region during winter (23 August to 5 October 2005) and summer (30 January to 14 March 2006). Both cruises departed from Punta Arenas, followed a sawtooth path out to 103°W, and concluded near Puerto Montt, crossing the SAF six times on each cruise (Figure 1). CTD station spacing was approximately 50 km. Each cruise included two diamond-patterned intensive surveys, one in the SAMW formation region and another at the SAF. The location of these intensive surveys varied by cruise depending on the position of the SAF. Both cruises were divided into three regions: (1) the region of shallow mixed layer depths (MLDs) equatorward of the deep SAMW mixed layers (north of 52°S and along Chile's coast); (2) the SAMW formation region, characterized by deep SAMW mixed layers north of the SAF (capped in summer); and (3) the region south of the SAF, the Polar Frontal Zone (PFZ), characterized by shallower, colder, and fresher mixed layers relative to the SAMW region. These regions are referred to as the gyre, SAMW formation, and PFZ regions in the paper, and are indicated in Figure 1.

[9] The 2005 austral winter and 2006 austral summer cruises collected 135 and 105 CTD/rosette/LADCP profiles, respectively, providing full depth profiles of temperature, salinity, oxygen, and velocity. All temperatures and densities listed in the remainder of the paper are potential temperatures and densities (σ_θ) referenced to the sea surface. Bottle samples (from a 24 bottle rosette in winter and a 36 bottle rosette in summer) were analyzed for dissolved oxygen, salinity, phosphate, nitrate, and silicate. These data were

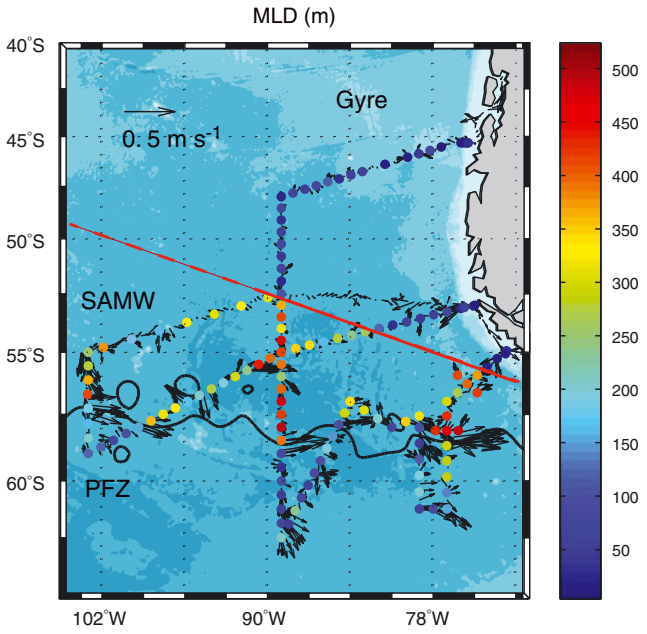

Figure 1. Mixed layer depth at CTD stations for the 2005 austral winter cruise extended from 0 m (blue) to 550 m (red). Underway ADCP currents (black arrows) averaged from 100 to 450 m are plotted every half hour along the cruise track. The mean Archiving, Validation, and Interpretation of Satellite Oceanographic data (AVISO) dynamic topography contour that most closely matched the SAF location in hydrography and ADCP data is also plotted (black line). The mean dynamic topography was calculated over the cruise period, 23 August to 5 October 2005. The three regions used in the OMP analysis are labeled on the map: gyre region (north of the red line), SAMW formation region (between the red line and the SAF), and the PFZ region (south of the SAF). The bathymetry is contoured at 1000 m intervals. The sections plotted in Figure 3 were taken along 89°W.

acquired and processed by Scripps Institution of Oceanography's Oceanographic Data Facility. Carbon parameters and chlorofluorocarbons were also collected during the winter cruise [*Hartin et al.*, 2011]. The lowered acoustic Doppler current profiler (LADCP), a 150 kHz RD Instruments Phase 3 broadband ADCP, provided full depth profiles from 60 m interpolated to a 20 m sampling interval.

[10] In addition to the cruise data, satellite altimetry and profiles from autonomous Argo floats were used to identify the large-scale conditions in the cruise region. Argo floats, of which the winter cruise deployed 13, have continuously sampled the cruise region since 2003, providing greater temporal coverage but reduced horizontal and vertical resolution relative to the cruises. Argo floats generally sample to a depth of 2000 m and measure temperature, salinity, and pressure at roughly 70 depth levels. Vertical sample spacing for most floats is less than 20 m to depths of 400 m, below which the spacing increases to 50 m. This study used 4994 Argo profiles collected in the cruise region. Argo data are available online at http://www.usgodae.org/argo/argo.html. Archiving, Validation, and Interpretation of Satellite Oceanographic data (AVISO) merged satellite topography was used to determine the mean position of the SAF during the cruises and to identify eddies; the "Reference" fields used in this study are available on weekly, 0.25° grids. AVISO is provided online at http://www.aviso.oceanobs.com.

3. Frontal Structure and Evidence of Cross-Frontal Exchange

[11] Argo profiles collected in the SAMW formation region north of the SAF freshened and cooled between the 27.0 and 27.3 kg m^{-3} isopycnals from 103°W to 73°W (Figure 2). For example, at 103°W, salinity along the

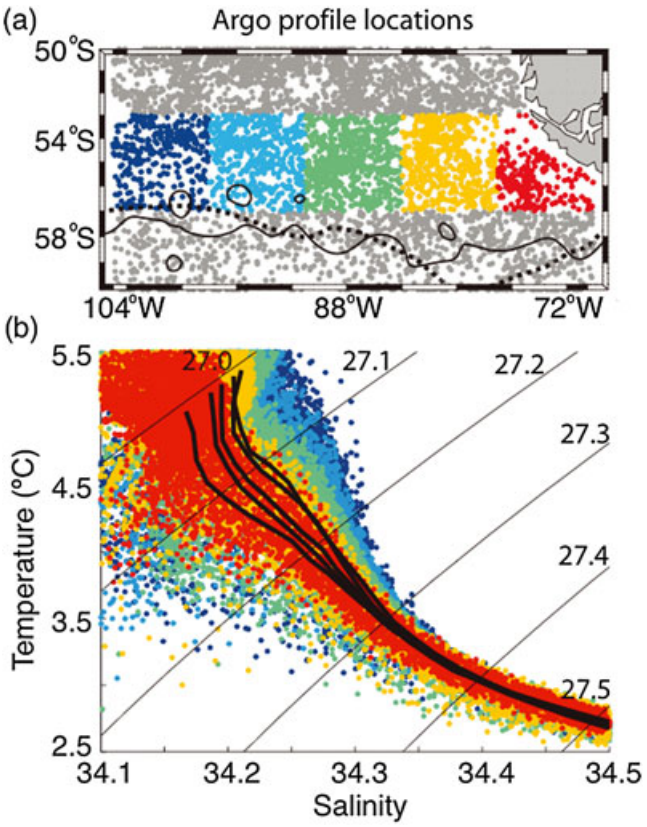

Figure 2. (a) Map of 4994 Argo profiles collected between January 2003 and February 2010. The profiles collected between 53 and 57°S were binned into five longitude groups; the bins, of 7° width, were centered at 73°W (red), 80°W (orange), 87°W (green), 94°W (light blue), and 101°W (dark blue). The latitude range of the binned profiles was generally north of the SAF, in the SAMW formation region. As for Figure 1, the mean AVISO dynamic topography contour that most closely matched the Subantarctic Front is also plotted (black line). The SAF defined by [*Orsi et al.*, 1995] is indicated by the dashed black line. (b) The temperature-salinity diagram of the binned profiles is plotted, where color again corresponds to each profile's longitude bin. The mean temperature and salinity values for each longitude bin are also plotted (black lines). The mean profiles cool and freshen to the east. Potential density is contoured at 0.1 kg m^{-3} intervals from 27.0 to 27.5 kg m^{-3}.

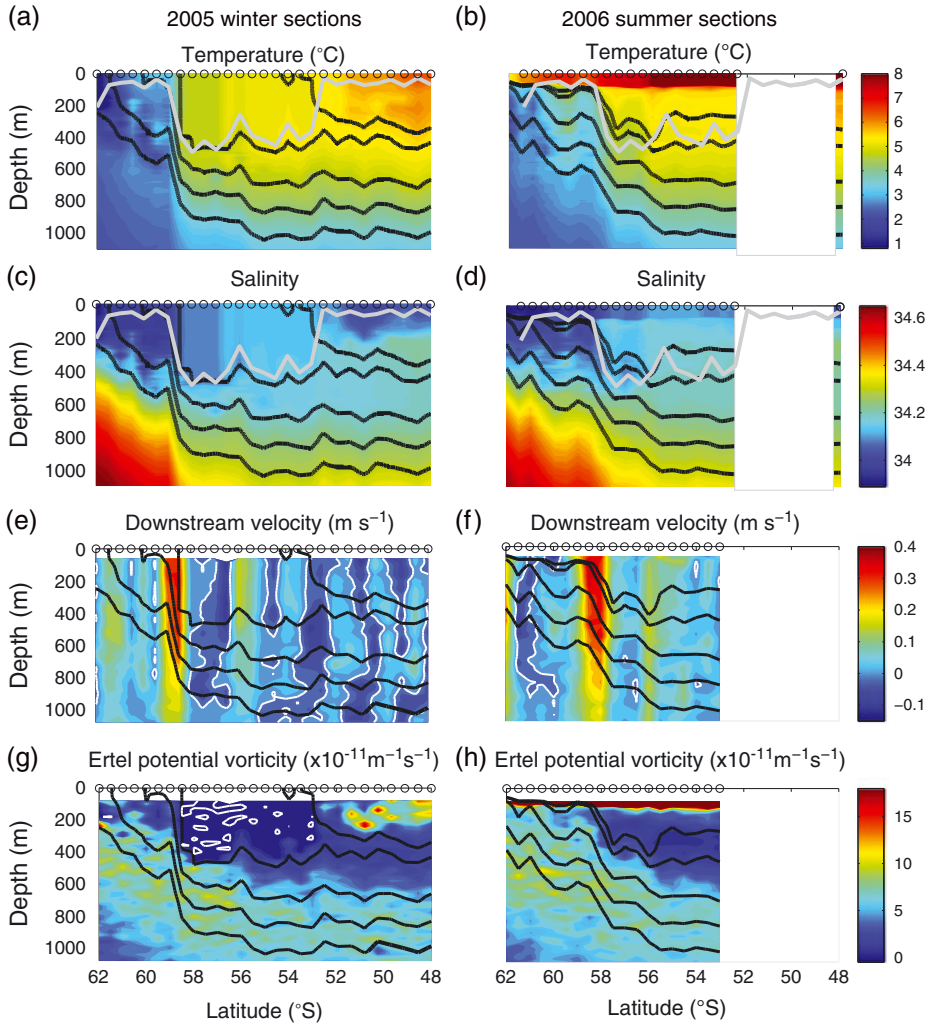

Figure 3. Sections of (a, b) potential temperature, (c, d) salinity, (e, f) downstream velocity, and (g, h) Ertel potential vorticity along 89°W from (left column) the 2005 austral winter cruise and (right column) the 2006 austral summer cruise. Potential density (bold black lines) is contoured for the 27.0, 27.02, 27.1, 27.2, and 27.3 kg m^{-3} isopycnals. The 2005 cruise MLD (grey line) is plotted in Figures 3a and 3c; it is shifted 0.6° north for the summer sections to match the location of the SAF in Figures 3b and 3d. White contours denote velocities and Ertel potential vorticities that are less than zero. The CTD station locations are denoted by circles at the surface. Poor weather conditions limited the northern CTD and LADCP profiles during the 2006 cruise.

27.2 kg m^{-3} isopycnal ranged from 34.22 to 34.3 psu and temperature ranged from 3.7 to 4.3°C. A narrower range of values was observed at 73°W; salinity ranged from 34.24 to 34.28 psu and temperature ranged from 3.8 to 4.2°C. Mean temperature and salinity properties along the 27.2 kg m^{-3} isopycnal changed from 34.28 psu and 4.12°C at 103°W to 34.26 psu and 3.97°C at 73°W, an along-front freshening of 0.02 psu and cooling of 0.15°C. SAMW mixed layers in the southeast Pacific attain their maximum winter potential density of approximately 27.05 kg m^{-3} just upstream of Drake Passage, near 75°W. The 27.2 kg m^{-3} isopycnal lies at a depth of approximately 800 m in the SAMW formation region. Therefore, much of the deep freshening and cooling observed by Argo was well beneath the mixed layer and hence cannot be attributed to local air-sea fluxes of heat and freshwater. Likewise, the 27.1, 27.2, and 27.3 kg m^{-3} isopycnals were beneath most of the wind-driven turbulent mixing identified by *Sloyan et al.* [2010], which was primarily concentrated in the upper 600 m. The cross-frontal exchange of cool, fresh waters from the PFZ is one possible mechanism for this along-front evolution of temperature and salinity properties in the SAMW region, both at depth and in the SAMW layer.

[12] Waters from the PFZ do not flow freely across the SAF, however, as both the PV structure of the SAF and kinematic effects of the ACC are likely to inhibit cross-frontal exchange. Sections along 89°W from the 2005 austral winter and 2006 austral summer cruises revealed a clear water mass separation between the SAMW formation region and the PFZ south of the SAF (Figure 3); there was a jump in temperature, salinity, and PV across the SAF. *Bower et al.* [1985], in a study of the Gulf Stream, found that cross-frontal mixing above 1800 m was primarily limited by the PV gradient. Similarly, *Beal et al.* [2006] found

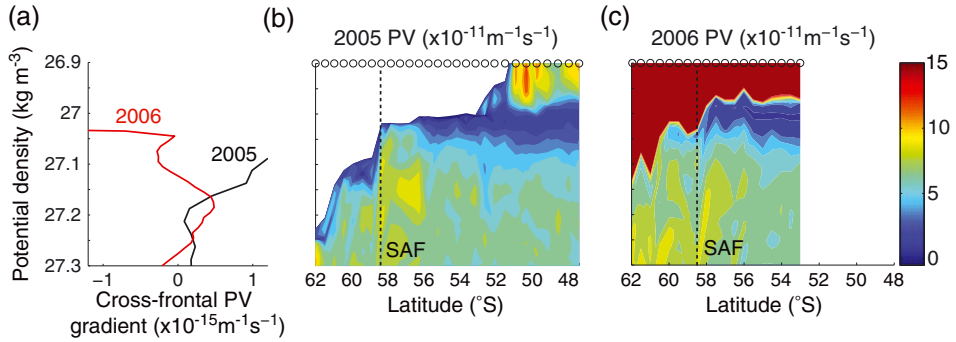

Figure 4. Potential vorticity (a) cross-frontal gradient and (b, c) sections contoured against potential density and latitude along 89°W. The cross-frontal PV gradient is calculated as the along-isopycnal difference in PV between the first CTD stations on either side of the SAF. The location of the SAF during each section is marked by the dashed line in Figures 4b and 4c.

that a high cross-stream gradient of PV was the dominant mechanism for water mass separation near the surface in the Agulhas Current. These current systems differ from the ACC observations in this study, in that their velocities often exceeded 1 m s^{-1}, whereas the maximum eastward velocities observed in this section of the ACC were approximately 0.5 m s^{-1}. Studies of the ACC have shown that higher eddy diffusivities, and presumably higher rates of cross-frontal exchange, were found in regions with lower cross-stream PV gradients and lower mean flows [*Marshall et al.*, 2006; *Shuckburgh et al.*, 2009; *Abernathey et al.*, 2010].

[13] To examine how the PV structure of the SAF might limit cross-frontal exchange in the southeast Pacific, we calculated the 2-D Ertel potential vorticity (EPV) using the LADCP velocity and CTD density profile data, following *Beal et al.* [2006]. EPV includes terms for the horizontal and vertical velocity shears that, because of the sloping isopycnals within the SAF, can significantly contribute to the vorticity normal to the isopycnals [*Beal et al.*, 2006; *Joyce et al.*, 2009]. The data were analyzed in a cross- and along-front coordinate system; the origin was located at the maximum vertically averaged current (averaged over the upper 800 m) and oriented so that the cross-front direction was normal to the maximum current vector. The density profiles were smoothed with a 20 m running mean and subsampled to match the LADCP sampling. The velocity and density fields were further smoothed with a 100 m running mean filter to remove small scale fluctuations. The EPV was then calculated using

$$\mathrm{EPV} = \frac{-1}{\rho}\left[f\frac{\partial \rho}{\partial z} + \left(\frac{\partial u}{\partial y}\frac{\partial \rho}{\partial z} - \frac{\partial u}{\partial z}\frac{\partial \rho}{\partial y} \right) \right], \qquad (1)$$

where ρ is the potential density, f is the Coriolis parameter, z is the vertical coordinate (positive downwards), y is the cross-front coordinate, and u is the along-front velocity. The first term on the right-hand side is the stretching term. The second and third terms are related to the horizontal and vertical shears, respectively. The SAMW mixed layers observed during the winter cruise were characterized by extremely low, and occasionally negative, EPV (Figure 3). The EPV was generally higher south of the SAF, where the water column was more stratified. An analysis of the EPV terms revealed that in this region of the ACC, the stretching term was more than an order of magnitude larger than the shear terms (not shown). The EPV terms related to the vertical shear of horizontal velocity only marginally contributed to the EPV because there was relatively little vertical velocity shear in the upper 1000 m in this section of the ACC, particularly compared to *Joyce et al.* [2009]'s observations of the Gulf Stream. We therefore retained only the stretching term, referred to as potential vorticity (PV) throughout the remainder of the paper, to analyze PV constraints on cross-frontal exchange.

[14] During the 2005 austral winter cruise, a strong cross-frontal PV gradient was observed along 89°W between the 27.05 and 27.175 kg m^{-3} isopycnals (Figures 4a and 4b). This gradient potentially limited exchange across the SAF. The jump in density between the lighter SAMW mixed layers north of the SAF and the denser PFZ mixed layers south of the SAF (Figure 3) suggested that cross-frontal exchange near the surface was also limited. The 2006 austral summer cruise featured a much smaller PV gradient across the SAF along the 27.05 kg m^{-3} isopycnal, perhaps indicating a pathway for cross-frontal exchange at the base of the SAMW layers (Figures 4a and 4c). The PV structure along 77°W was similar to the winter section along 89°W, suggesting limited exchange above the 27.175 kg m^{-3} isopycnal. Along the farthest west section at 103°W, larger PV gradients were observed for densities greater than 27.05 kg m^{-3}.

[15] Kinematic effects can also limit cross-frontal exchange above a current's "steering level," the depth at which the current speed is equal to the phase speed of meanders in the current [*Owens*, 1984; *Beal et al.*, 2006; *Abernathey et al.*, 2010]. *Abernathey et al.* [2010] calculated a phase speed of ~2 cm s^{-1} and a "steering level" of 2000 m for the ACC. Following the approach of *Abernathey et al.* [2010], we constructed a Hovmöller diagram of AVISO altimetric sea surface height in the study region to estimate the meander phase speed of the ACC (not shown). The observed phase speed of ~2.8 cm s^{-1} corresponded to a "steering level" of approximately 1500 to 2000 m (the depth at which the mean current speed from our survey matched the phase speed); thus, kinematic effects could also limit cross-frontal exchange in all of the isopycnals considered in our analysis, including SAMW. This "steering level" was similar to those reported by

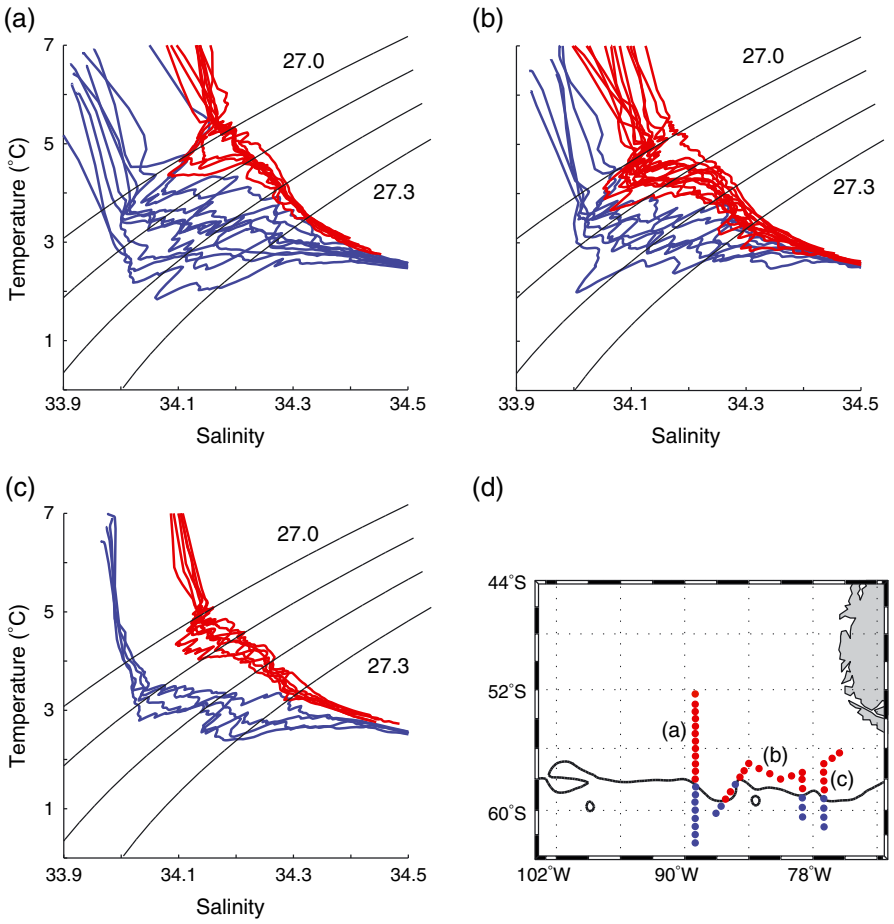

Figure 5. Temperature-salinity diagrams for three regions from the 2006 austral summer cruise; (a) 89°W, (b) zigzag centered at 83°W, and (c) 77°W. (d) The profile locations for each region are shown. Red corresponds to profiles in the SAMW formation region and blue corresponds to profiles in the PFZ. Potential density (black lines) is contoured at 0.1 kg m^{-3} intervals from 27.0 to 27.3 kg m^{-3} in Figures 5a–5c.

Smith and Marshall [2009]. The small PV gradients beneath the 27.2 kg m^{-3} isopycnal, the proximity to the "steering level," as well as the convergence of Argo temperature-salinity relationships at this density in Figure 2, suggest that cross-frontal transport and mixing is much less limited at densities greater than 27.2 kg m^{-3}.

[16] Despite these potential barriers to exchange, numerous specific instances of cross-frontal exchange were observed during both cruises. Rather than cataloging all of the intrusions, we present a few examples representative of both cruises. The most significant subsurface intrusion in the SAMW formation region was observed during the 2006 austral summer cruise along 89°W just north of the SAF, at approximately 400 m depth (Figures 3b and 3d). This relatively fresh and cold feature impinged on capped SAMW layers and corresponded to a minimum cross-frontal PV gradient along the 27.05 kg m^{-3} isopycnal (Figures 4a and 4c). The intrusion, more than 100 m thick, was 0.6°C cooler and 0.125 psu fresher than the nearby SAMW; the temperature-salinity characteristics of the 89°W intrusion are shown in Figure 5. Similar features were observed in the along-front section that paralleled the SAF in the SAMW formation region and in the SAF crossing at 77°W; all featured intrusions near the base of the SAMW layers, between approximately the 27.0 and 27.1 kg m^{-3} isopycnals (Figure 5). A similar intrusion was observed in the same region during the 2005 austral winter cruise; it was 0.5°C cooler and 0.04 psu fresher than the surrounding waters, and 80 m thick (visible in the temperature and salinity profiles from 79°W in Figure 6). *Chereskin et al.* [2010] found that SAF meanders in the Southeast Pacific were quasi-stationary, maintaining their position relative to the deep SAMW mixed layers on seasonal time scales, which could allow for the formation of such large, long-lived features.

[17] Many less dramatic, smaller intrusions were observed at the six frontal crossings during the 2005 austral winter cruise, particularly in the layers immediately below the SAMW mixed layers, generally between the 27.0 and 27.1 kg m^{-3} isopycnals (Figure 6). The lightest intrusions were observed along 103°W, where the densest SAMW mixed layers reached 27.0 kg m^{-3}. At 77°W, the maximum SAMW densities increased to approximately 27.04 kg m^{-3}, and the densities of the intrusions increased correspondingly. While the temperature and salinity anomalies associated with these intrusions were similar to the significant intrusion observed in 2006, the 2005 intrusions

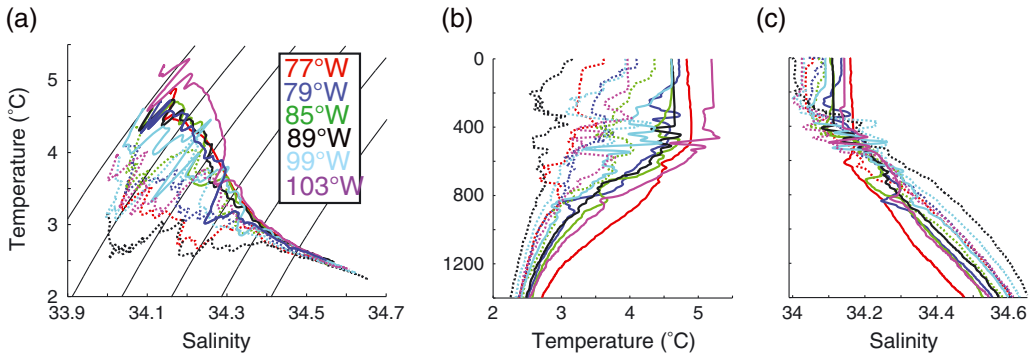

Figure 6. (a) Temperature-salinity diagram. (b, c) Profiles from paired stations spanning the SAF from all of the front crossings during the 2005 austral winter cruise. Dashed profiles are from south of the SAF core. Potential density is contoured at 0.1 kg m^{-3} intervals from 27.0 to 27.5 kg m^{-3} in Figure 6a.

were thinner, rarely exceeding a thickness of 50 m. Fewer intrusions into the SAMW mixed layers were observed during the 2005 austral winter cruise than the 2006 summer cruise, perhaps because any intrusions would be quickly incorporated into the SAMW by convection- and wind-driven turbulent mixing in the mixed layer [*Sloyan et al.*, 2010; *Holte et al.*, 2012]. Similarly, the large cross-frontal PV gradient observed during the 2005 austral winter cruise (Figure 4) could limit the formation of intrusions.

[18] The salinity of the shallow (approximately 80 m) summer mixed layer in the SAMW formation region also suggests the importance of cross-frontal exchange in the form of Ekman transport (Figure 3). *Lenn and Chereskin* [2009] found that the mean Ekman depth (∼100 m) was shallower than the mean mixed layer depth (∼120 m) in Drake Passage, consistent with our interpretation of a shallow Ekman layer in the summer observations. The most saline summer mixed layers along 89°W, 34.11 psu, were observed in the middle of the SAMW formation region, at 55°S; the mixed layer was approximately 0.05 psu fresher than the capped SAMW beneath it. Closer to the SAF, the summer mixed layer freshened to 34.03 psu, increasing the salinity difference between the capped SAMW and the summer mixed layer to 0.1 psu. The vertical extent and salinity anomaly (relative to the SAMW) of the summer mixed layer were similar to the intrusions described above. The meridional salinity pattern suggests that surface waters from south of the SAF penetrated to nearly 3° north of the SAF during summer, though some of the freshening in the surface layer was likely due to local precipitation. In winter, mixing the fresher, 80 m surface layer with the 400 m of SAMW below it would decrease the salinity of the SAMW by approximately 0.01 to 0.02 psu. No evidence of Ekman transport was observed during the winter cruise, again because it would likely be quickly mixed into the SAMW mixed layers. Quantifying the relative importance of intrusions and Ekman transport was difficult with our data set.

[19] Besides intrusions and Ekman cross-frontal exchange, a cold core eddy was observed in the SAMW formation region at approximately 96°W and 56°S during the 2005 austral winter cruise. The eddy's cyclonic rotation was captured by the LADCP (Figure 1). The eddy's mixed layer was 0.3°C cooler and 0.03 fresher than the surrounding SAMW mixed layers, and more than 150 m shallower. As the eddy decayed, the polar water that it was transporting would be dispersed into the SAMW formation region.

[20] To summarize, during the two cruises numerous intrusions, Ekman transport, and eddies frequently overcame the SAF's PV barrier to transport PFZ water into the SAMW formation region. Many of the intrusions were near the maximum densities of the winter SAMW mixed layers. Ekman transport likely produced the fresh layer that capped the SAMW during the summer cruise.

4. Optimum Multiparameter Analysis

4.1. Method and Setup

[21] We employed an optimum multiparameter (OMP) analysis to examine the cumulative effect of cross-frontal exchange on water properties in the SAMW formation region. OMP analysis, originally developed by *Tomczak and Large* [1989], is an inverse method for calculating the relative contributions of various user-defined source waters to a water sample. We used a MATLAB OMP package provided online by Johannes Karstensen at http://www.ldeo.columbia.edu/∼jkarsten/omp_std/. OMP analyses have been used to assess water mass mixing in the thermocline in the Eastern Indian Ocean [*Tomczak and Large*, 1989] and the Atlantic Ocean [*Poole and Tomczak*, 1999], to examine shelf waters in the Ross Sea [*Budillon et al.*, 2003], and to look at water masses in Southern Drake Passage [*Frants et al.*, 2012]. *Klein and Tomczak* [1994] used OMP analysis to study the diapycnal mixing of North and South Atlantic Central Water.

[22] OMP analysis is implemented by solving an overdetermined system of linear equations, written as

$$\mathbf{Gx} - \mathbf{d} = \mathbf{r}, \tag{2}$$

where **G** is a matrix defining the source water properties (in our case, the temperature, salinity, silicate, nitrate, phosphate, and oxygen levels of the three types of source water), **d** is the vector of observed properties for all of the cruise CTD stations, **x** is the solution vector giving the relative contribution of each source water at each CTD station, and **r** is the residual. Mass was added as an additional constraint; it was set to one for the source waters and the CTD stations and was unitless. The mass balance

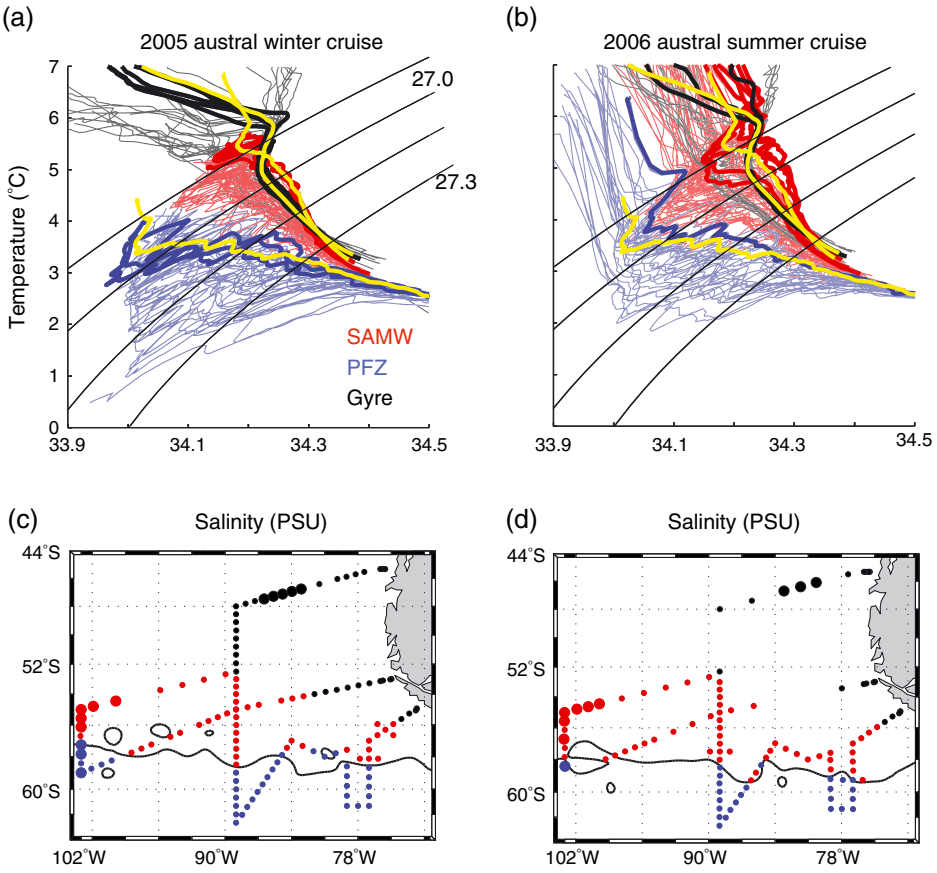

Figure 7. (a, b) Temperature-salinity diagrams. (c, d) Maps of 2005 austral winter and 2006 austral summer cruise CTD profiles. The profiles and their locations are colored by region. Each cruise was divided into three regions, as described in section 2: SAMW region (red), PFZ (blue), and gyre region (black). In summer, the SAMW mixed layers were capped by a shallow mixed layer. Profiles used to calculate the OMP source water properties and the property weights are marked by bold profiles in Figures 7a and 7b and large dots in Figures 7c and 7d. In Figures 7a and 7b, the multiyear mean profiles of the source water groups are plotted in yellow, and the potential density is contoured at 0.1 kg m^{-3} intervals from 27.0 to 27.3 kg m^{-3} intervals. In Figures 7c and 7d, the mean AVISO dynamic topography contour that most closely matched the SAF location in hydrography and ADCP data during each cruise is also plotted (black line). The mean dynamic topography was calculated over each cruise period.

residual was used to gauge the uncertainty of the result. Mass residuals less than or equal to 0.05 were considered acceptable [*Tomczak and Large*, 1989; *Poole and Tomczak*, 1999; *Budillon et al.*, 2003]. Standard OMP analysis assumes that the source water properties defined in **G** are conserved, which is acceptable if the study region is small, and the source waters are fairly close together [*Leffanue and Tomczak*, 2004]. Including the Redfield ratio [*Redfield et al.*, 1963], which accounts for the consumption of nutrients and oxygen, allows OMP analysis to be expanded to basin scales, as in *Poole and Tomczak* [1999]. As our analysis was much smaller than basin-scale, we did not include a Redfield constraint.

[23] Our three source waters included an upstream profile representative of the western SAMW region and a profile in the PFZ south of the SAF to represent the water crossing the front. The third source water represented subtropical gyre water and allowed the OMP analysis to resolve samples collected north of the SAMW formation region. For our OMP analysis, the source water properties were calculated by taking the mean of groups of profiles with similar temperature-salinity characteristics from both the 2005 and 2006 cruises. For example, five profiles from the 2005 cruise (121–125) and three profiles from the 2006 cruise (233–235), all centered near approximately 84°W, 47°S, were used to calculate the gyre water properties; the mean of these eight profiles represented the gyre source water properties. The source water properties used in the OMP analysis were therefore the same whether we were analyzing data from the 2005 or the 2006 cruise. Three profiles from the 2005 cruise (74, 75, and 77) and one profiles from the 2006 cruise (213) were used to calculate the PFZ water properties; the profiles were collected near 103°W, 58°S. The upstream SAMW properties were derived from five profiles from the 2005 cruise (68–72) and six profiles from the 2006 cruise (204–208, 210), all centered near approximately 103°W, 55°S. The mean source water profiles and the groups of profiles used to calculate the source water profiles, as well as the profile locations, are shown in Figure 7.

Table 1. Definitions of Source Waters Used in the OMP Analyses[a]

Source Water	Temperature	Salinity	Oxygen	Nitrate	Silicate	Phosphate	PV
27.0–27.1 σ_θ							
Upstream SAMW	5.21	34.23	248	25.6	14.9	1.8	6.06
PFZ	3.84	34.05	293	24.9	11.7	1.7	5.92
Gyre	5.30	34.23	255	25.0	10.7	1.7	3.21
27.1–27.2 σ_θ							
Upstream SAMW	4.58	34.28	220	29.1	24.5	2.0	7.53
PFZ	3.37	34.10	268	27.9	19.2	1.9	8.10
Gyre	4.48	34.26	226	29.1	21.7	2.0	6.58
27.2–27.3 σ_θ							
Upstream SAMW	3.90	34.31	209	31.1	34.3	2.1	7.76
PFZ	3.40	34.24	224	31.1	32.6	2.1	7.24
Gyre	3.91	34.30	202	31.8	33.5	2.2	7.19

[a]Temperature is given in °C. Oxygen is given in mmol L^{-1}. Nutrients are given in mmol kg^{-1}. PV, in this case the stretching term, is given in 10^{-11} m^{-1} s^{-1}.

[24] The PFZ possessed the widest range of temperature-salinity profiles (Figure 7). In general, profiles from the PFZ cooled and freshened to the east and to the south. Profiles close to the SAF were probably most representative of the water crossing the SAF. For the 2005 and 2006 cruises, we selected PFZ profiles along 103°W, the westernmost section of the cruise. Only one profile from the 2006 austral summer cruise was collected south of the SAF at 103°W. Upstream profiles in the SAMW region, near 103°W, exhibited salinity maxima centered on the 27.1 kg m^{-3} isopycnal, a feature that eroded by 89°W. Profiles with these subsurface salinity maxima were selected as the SAMW region source waters, as these features formed extremes on the temperature-salinity diagrams. The subtropical gyre region was characterized by two groups of profiles on both cruises. One group, fresher between the 27.0 and 27.3 kg m^{-3} isopycnals, was observed closer to Chile's coast; the other group was observed on the sections north of 52°S. The gyre source water properties were calculated with profiles from the latter group, as this was more likely representative of the gyre; the fresher branch could be the result of mixing with water from the PFZ or SAMW region. Near the surface, the freshening in the waters near Chile was likely due to local precipitation and runoff.

[25] The OMP analysis was conducted for two primary isopycnal ranges, 27.1–27.2 kg m^{-3} and 27.2–27.3 kg m^{-3}, for both the 2005 and 2006 cruises. Isopycnals in these ranges displayed the greatest downstream changes in temperature and salinity characteristics (Figure 2) and were not directly influenced by air-sea fluxes. Our OMP analysis was formulated as an isopycnal analysis with no allowance for diapycnal exchange, though diapycnal exchange was likely small for these isopycnals, especially north of the SAF [*Sloyan et al.*, 2010]. An OMP analysis was also run for the 27.0–27.1 kg m^{-3} isopycnal range for the 2006 austral summer cruise. These lighter isopycnals outcropped during winter, particularly south of the SAF, but provided a sense of the transport closer to the winter mixed layer. All of the OMP runs used CTD temperature, CTD salinity, CTD oxygen, and bottle silicate, nitrate, and phosphate as properties. An additional set of five repeat runs included PV as a property. All bottle data falling within the isopycnal ranges were averaged together to form the isopycnal values used in the analysis. The property values for the OMP runs are shown in Table 1.

[26] A weight matrix, **W**, accounted for each property's varying ability to distinguish the source waters in each water sample. For example, if the nitrate distribution in all of the water samples was largely random, then nitrate should not have been given much weight in the OMP analysis. Weights were calculated for each property following *Tomczak and Large* [1989],

$$W_j = \frac{\sigma_j^2}{\delta_j \mathrm{max}}, \tag{3}$$

where j indexes the property, $\delta_{j\mathrm{max}}$ is the largest source water variance for property j, and σ_j represents the ability of property j to resolve differences in source water content. The source water variance, δ_j, was calculated separately for each source water; we simply computed the variance of each group of profiles used to define the source water properties. The largest variance of the source water groups was used as $\delta_{j\mathrm{max}}$. For smaller variances, the source water property was representative of nearby profiles, whereas higher variances signaled that there was considerable property variability near the source water and that it might therefore not be useful in the analysis. The ability of property j to resolve differences in source water content, σ_j, is represented by the expression

$$\sigma_j = \sqrt{1/n \sum_{i=0}^{n} \left(G_{ij} - \bar{G}_j\right)^2}, \tag{4}$$

where G_{ij} is an element of **G** (property j, source water i) and $\bar{G}_j$ is the mean value of property j for the n source waters. Traditionally, σ_j was interpreted as a measure of how useful property j was at resolving the source waters; if the source waters had very different values of property j, then it would be useful for resolving the source water content in each of the water samples, and correspondingly have a large σ_j and weight.

[27] The weights are shown in Table 2. The weights were similar to weights used by *Budillon et al.* [2003] and *Frants et al.* [2012], in that temperature, salinity, and oxygen were assigned considerably larger weights than the nutrients.

Table 2. Weights Used in the OMP Analyses

Property	27.0–27.1	27.1–27.2	27.2–27.3
Temperature	105.9	28.9	14.3
Salinity	80.1	22.6	12.7
Oxygen	22.4	22.0	19.3
Nitrate	7.6	6.1	4.9
Silicate	10.3	7.0	2.4
Phosphate	7.4	1.6	4.2

As in other studies (e.g. *Kerr et al.* [2009]), oxygen was a useful parameter for distinguishing the source waters, and its weight was similar to the large weights given to temperature and salinity. The weights for phosphate and nitrate were small because these properties displayed little variation between source waters. The PV and mass balance weights were arbitrary; as other studies have done, we employed the temperature weight for mass and PV.

[28] Following *Poole and Tomczak* [1999] and *Hinrichsen and Tomczak* [1993], a sensitivity analysis was conducted to determine the robustness of the results to variations of the source water properties. For the sensitivity analysis, the OMP analysis was repeated with a simulated **G**, which defined the source water properties, composed of properties generated randomly from normal distributions with the same means and variances as the original groups of source water profiles. **G** was randomly generated 50 times for each of the three isopycnal ranges, and run through the analysis to produce simulated OMP runs. The root-mean-square (RMS) error of each station was calculated by taking the standard deviation of the difference between the SAF water content of the standard and simulated OMP runs. The RMS error was then spatially averaged over all of the cruise stations (Table 3).

4.2. Results

[29] The OMP analysis revealed that the fractional content of PFZ water in the SAMW formation region increased in the along-front direction between the 27.1 and 27.3 kg m^{-3} isopycnals (Figure 8). Profiles from the cruises' eastern sections, near 77°W, exhibited greater fractional contents of PFZ water than upstream profiles. This was most evident in the 27.1–27.2 kg m^{-3} isopycnal range for both cruises. The 27.2–27.3 kg m^{-3} PFZ water fractional contents were noisier than for the other ranges, perhaps because exchange was less limited for denser portions of this range (as evidenced by the convergence of properties in this isopycnal range in Figure 2). However, both distributions of PFZ fractional content in this density range suggested the same pattern of increased downstream PFZ concentrations within 4° latitude of the SAF. Profiles at or immediately south of the SAF had high concentrations of PFZ water, as expected. Profiles farther south in the PFZ had unrealistically large mass balance residuals, as the source waters were not defined to resolve these profiles.

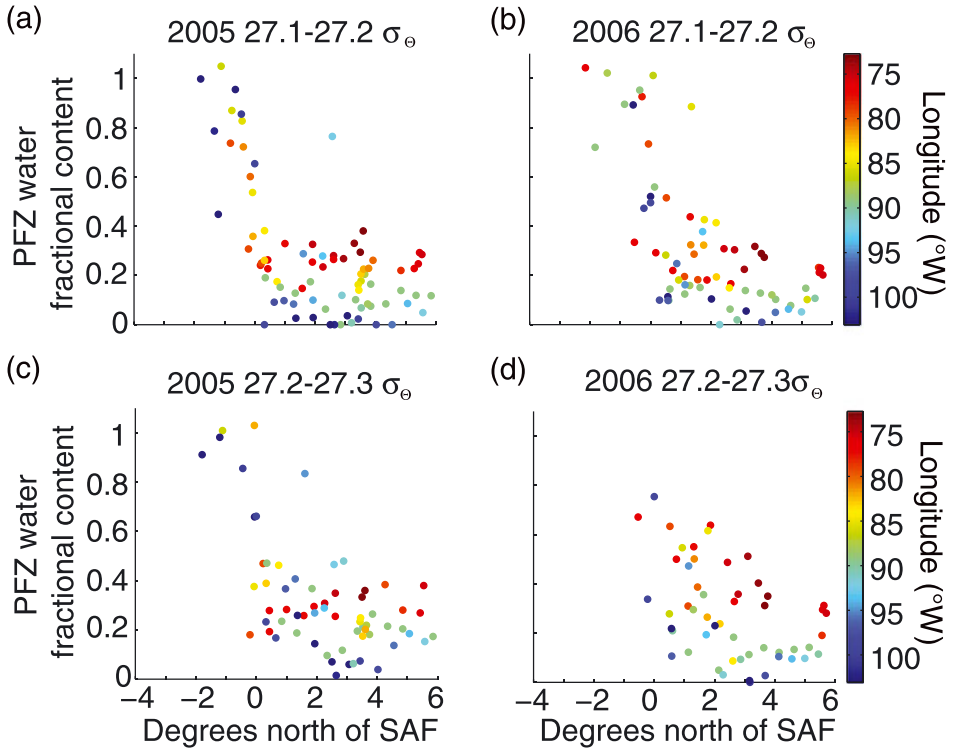

Figure 8. OMP-derived fractional content of PFZ water for (a, c) the 2005 austral winter and (b, d) 2006 austral summer cruises performed in two potential density ranges, 27.1–27.2 kg m^{-3} and 27.2–27.3 kg m^{-3}. These OMP runs did not include PV as a property. The fractional content of PFZ water is plotted against distance from the SAF, which is calculated by interpolating the SAF latitudes observed in hydrography and ADCP data to the profile longitudes. Color corresponds to profile longitude, from 103°W (blue) to 73°W (red).

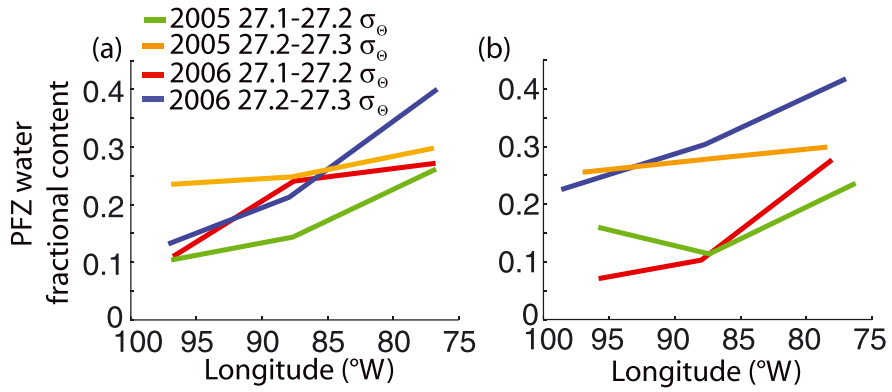

Figure 9. Mean PFZ water fractional content for the OMP runs averaged into zonal bins for (a) standard OMP analysis and (b) OMP analysis that included PV as a property. The OMP runs were performed for two potential density ranges for the 2005 austral winter cruise: 27.1 to 27.2 kg m^{-3} (green) and 27.2 to 27.3 kg m^{-3} (orange). The same isopycnals were used for the 2006 austral summer cruise (27.1 to 27.2 kg m^{-3} (red) and 27.2 to 27.3 kg m^{-3} (blue)). For each run, all of the stations within 6° of the front were averaged into bins from 103° to 90°W, 90° to 83°W, and 83° to 75°W. Each profile's distance from the SAF was calculated by interpolating the SAF latitudes observed in hydrography and ADCP to the profile longitudes.

[30] To estimate the "rate" of cross-frontal exchange, the mean PFZ water fractional content north of the SAF was calculated for three zonal bins (103°W to 90°W, 90°W to 83°W, and 83°W to 75°W) (Figure 9). The 27.1–27.2 kg m^{-3} isopycnal range exhibited an along-front increase in PFZ water fractional content of 0.12 every 15° of longitude in both 2005 and 2006. The PFZ water fractional content of the 2006 27.2–27.3 kg m^{-3} isopycnal range increased the most, by 0.2 over 15°. Water samples from 2005 in the SAMW region between the 27.2 and 27.3 kg m^{-3} isopycnals exhibited the smallest along-front increase in PFZ water fractional content, 0.05. Averaging all of the binned OMP results, we found that the fractional content of PFZ water in the SAMW formation region increased by approximately 0.13 for every 15° of longitude. The OMP analysis suggests that the rate of cross-frontal exchange increased slightly in the longitude bins closest to Drake Passage, as evidenced by the greater change of PFZ fractional content over 85°W to 75°W relative to 95°W to 85°W (Figure 9). As noted in *Sokolov and Rintoul* [2009a], this increased exchange could be due to the convergence of the ACC fronts near Drake Passage.

[31] Adding PV as a property did not substantially alter the results (Figure 9). The "rate" of cross-frontal exchange was smaller in both isopycnal ranges for the 2005 cruise, most likely because there was such a strong PV gradient across the SAF in these isopycnal ranges during the winter cruise (Figure 4); over 15° longitude, the PFZ water fractional content increased by 0.06 for the 27.1–27.2 kg m^{-3} isopycnal range and 0.04 for the 27.2–27.3 kg m^{-3} isopycnal range. With PV, the 2006 isopycnal ranges exhibited along-front PFZ water fractional content increases of

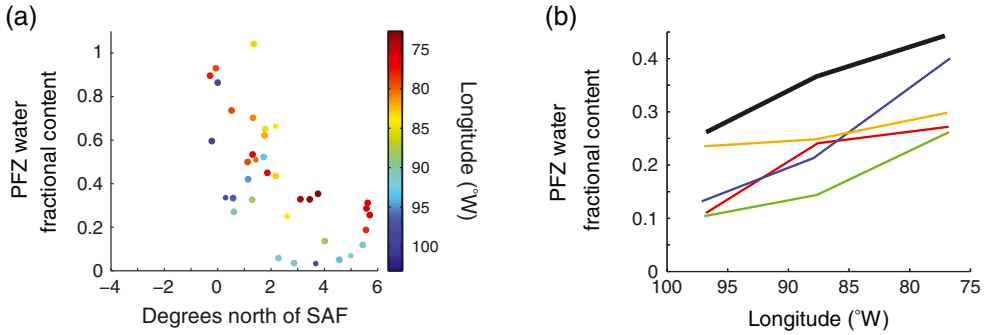

Figure 10. (a) Fractional content of PFZ water for the 2006 austral summer cruise performed in the potential density range 27.0–27.1 kg m^{-3}. The fractional content is plotted against distance from the SAF, which is calculated by interpolating the SAF latitudes observed in hydrography and ADCP data to the profile longitudes. Color corresponds to profile longitude, from 103°W (blue) to 73°W (red). (b) The mean values of fractional content of PFZ water for the 2006 potential density range 27.0 to 27.1 kg m^{-3} (black) was averaged in zonal bins as in Figure 9. The mean values for the other density ranges are plotted as in Figure 9.

Table 3. Mean Root Mean Square (RMS) Error of Fractional PFZ Water Content for 50 Simulations Where the Properties of All Three Source Waters Were Varied According to Their Respective Means and Variances[a]

2005 27.1–27.2	2005 27.2–27.3	2006 27.0–27.1	2006 27.1–27.2	2006 27.2–27.3
3.4%	5.2%	5.8%	4.8%	4.3%

[a]The mean was calculated over all CTD stations.

0.17 (27.1–27.2 kg m^{-3}) and 0.13 (27.2–27.3 kg m^{-3}) over a longitudinal distance of 15°.

[32] The OMP results for the 2006 27.0–27.1 kg m^{-3} isopycnal range also revealed an along-front increase in the fractional content of PFZ water in the SAMW formation region, mirroring the results of the denser isopycnals (Figure 10a). This near-surface layer also featured a variation in PFZ water content as a function of latitude; at a given longitude, the largest PFZ water content was found closest to the SAF and decreased farther north. This shallow layer exhibited a greater final mean PFZ water content at 77°W than any of the other runs (Figure 10b). Estimating the "rate" of exchange as described for the denser isopycnal ranges, we found that the PFZ water content increased by approximately 0.15 for every 15° of longitude in this lighter density range. This increased exchange was perhaps not surprising, given that the largest downstream changes in temperature and salinity in Argo profiles were observed between 27.0 and 27.1 kg m^{-3} isopycnals (Figure 2).

[33] The results of the sensitivity analysis are displayed in Table 3. Varying the source water properties produced RMS errors of PFZ water fractional concentrations of up to 6% in the SAMW region, suggesting that the results are robust to source water property variations. Therefore, the result was not due to a fortuitous selection of source waters, but rather would hold if we selected any of the nearby stations as source waters.

5. Discussion

[34] Argo profiles collected in the SAMW formation region north of the SAF in the southeast Pacific Ocean exhibited an along-front evolution, becoming fresher and cooler to the east between the 27.0 and 27.3 kg m^{-3} isopycnals (Figure 2). This density range included the densest SAMW and also Antarctic Intermediate Water. The along-front evolution could not have been accomplished by simple vertical mixing as the profiles were advected downstream, as this would have eroded the salinity minimum feature at approximately 27.1 kg m^{-3}, not maintained it. Likewise, the densest SAMW winter mixed layers in this region reach 27.04 kg m^{-3}, so much of this density range was insulated from the influence of local surface forcing. This study explored cross-frontal exchange as a possible mechanism for this along-front evolution. The cross-frontal exchange was likely accomplished by a combination of Ekman transport (e.g., *Dong et al.* [2008]; *Ito et al.* [2010]), meanders in the SAF (e.g., *Bower and Rossby* [1989]), intrusions (e.g. *Park and Gambéroni* [1997]), eddies (e.g., *Ansorge et al.* [2006]; *Sokolov and Rintoul* [2009b]), frontal convergence (e.g., *Sokolov and Rintoul* [2009a]), and current shear (e.g., *Abernathey et al.* [2010]).

[35] The steep isopycnals, PV structure, and kinematic effects of the SAF generally act to limit exchange in the upper ocean, as evidenced by the clear separation of surface waters north and south of the SAF (Figure 3). Two cruises in the southeast Pacific Ocean in 2005 and 2006 were designed to sample the SAMW formation region north of the SAF and the colder, polar waters to the south. An analysis of the PV along 89°W revealed a strong PV gradient across the SAF that could have acted as a barrier to exchange above the 27.2 kg m^{-3} isopycnal, to a depth of roughly 800 m. Likewise, exchange was likely limited above the ACC's "steering level," estimated to be 1500 m in this region.

[36] Regardless of such constraints, numerous instances of cross-frontal exchange were observed during both cruises, including large intruding structures with longitudinal dimensions of approximately 15° (Figure 5) and numerous intrusions at the base of the winter SAMW mixed layers (Figure 6). Ekman transport of polar water across the SAF likely contributed to the fresh surface layer that capped the SAMW during the summer cruise (Figure 3d). A cold-core eddy was observed in the SAMW formation region at 96°W during the winter cruise (Figure 1). Together, these features suggest that PFZ water can overcome the barriers to exchange through a number of mechanisms to be injected into the SAMW formation region. *Beal et al.* [2006] found that cross-frontal mixing events in the Agulhas were primarily driven by mesoscale features, such as meanders and shear-edge eddies, even though kinematic steering and PV gradients inhibited cross-frontal mixing near the surface.

[37] With such a multitude of mechanisms for cross-frontal exchange, we utilized an OMP analysis to estimate the fractional content of PFZ water in CTD profiles from the SAMW formation region. The OMP analysis did not distinguish between cross-frontal mixing and cross-frontal transport, but instead provided an estimate of the cumulative effect of cross-frontal exchange in the SAMW formation region. The OMP analysis revealed an along-front increase in PFZ water fractional content in the SAMW formation region at isopycnals between 27.0 and 27.3 kg m^{-3}. The fractional content of PFZ water increased along-front by approximately 0.13 for every 15° of longitude, even when PV was included as a property, between the 27.1 and 27.3 kg m^{-3} isopycnals (Figure 9). For the 27.0 to 27.1 kg m^{-3} isopycnal range, the fractional content of PFZ water increased along-front by approximately 0.15 for every 15° of longitude. Assuming an average downstream velocity of 0.05 m s^{-1} (Figure 3), the SAMW layers would be advected 15° in 200 days. Therefore, in this region of the southeast Pacific, the cross-frontal exchange diagnosed by the OMP analysis represented the cumulative exchange integrated over multiple seasons. For this reason, the OMP analysis results at individual CTD stations could not be directly tied to specific instances of cross-frontal exchange observed during the cruises.

[38] We used Argo profiles as an independent data set to verify the cross-frontal exchange diagnosed by the OMP

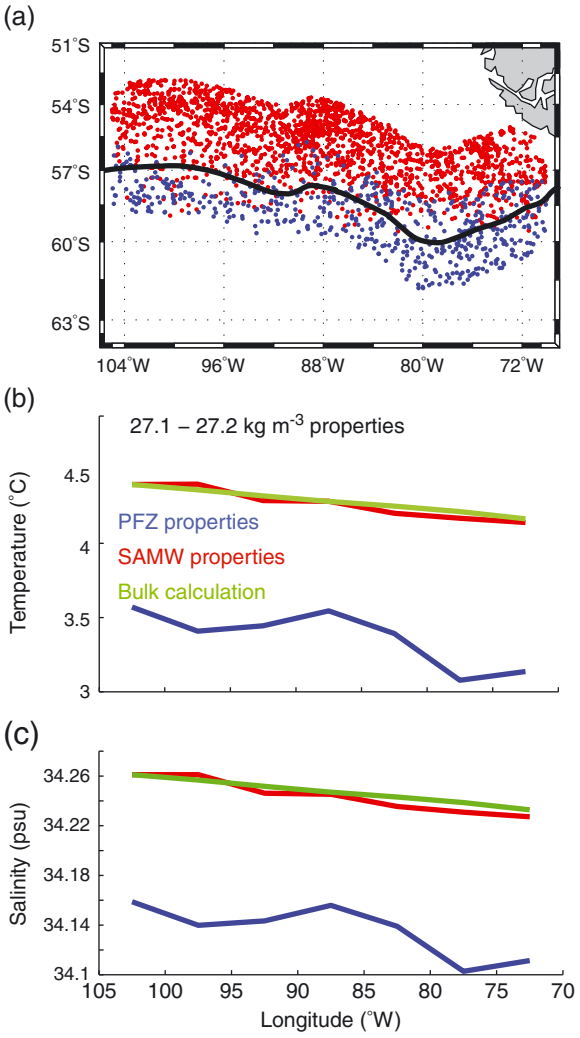

Figure 11. (a) Map of Argo profiles collected within 4° north and 2° south of the *Orsi et al.* [1995] SAF (black line). Profiles warmer and saltier than 3.55°C and 34.27 psu between the 27.2 and 27.3 kg m^{-3} isopycnals were assumed to be from the SAMW region (red dots), whereas cooler and fresher profiles were assumed to be from the PFZ (blue dots). (b and c) The along-front temperature and salinity properties of profiles from the SAMW region (red lines) and the PFZ region (blue lines), averaged over the 27.1 to 27.2 kg m^{-3} isopycnal range and in longitude bins of 5° width, are plotted. (b and c) The green lines are the result of a simple bulk calculation; SAMW-region properties, initialized using the westernmost bin, were evolved downstream by mixing in a 0.043 fraction of PFZ water every 5°.

analysis. Argo profiles from the SAMW region were binned by longitude and averaged over the 27.1 to 27.2 kg m^{-3} isopycnal range; as expected, the mean profiles cooled and freshened downstream (Figure 11). We initialized a bulk calculation with temperature and salinity values from the westernmost Argo bin, 105°W to 100°W. For every 5° of longitude, the temperature and salinity were evolved by mixing in a 0.043 fraction of PFZ water. The 0.043 fraction of PFZ water represented the OMP analysis' average rate of cross-frontal exchange. The PFZ water properties were derived from Argo profiles south of the SAF. The downstream evolution of temperature and salinity in the bulk calculation closely tracked the downstream evolution of temperature and salinity observed by Argo (Figures 11b and 11c), thus contributing to our confidence in the rate of cross-frontal exchange diagnosed by the OMP analysis of cruise data.

[39] What are the implications for SAMW if this pattern of cross-frontal transport carries into the mixed layer? We conducted another simple bulk calculation with SAMW mixed layer properties from the 2005 austral winter cruise to determine if the OMP-diagnosed cross-frontal exchange could account for the observed along-stream evolution of SAMW. As noted in *Holte et al.* [2012], the SAMW mixed layers cooled and freshened zonally over the 1500 km covered by the cruise; their density increased by approximately 0.05 kg m^{-3}. The similarity of the OMP results at all subsurface isopycnal levels tested here, including 27.0–27.1 kg m^{-3}, gave us confidence that similar transport might occur near the mixed layer. The bulk calculation was initialized with SAMW winter mixed layers collected on the 2005 cruise along 103°W. Using the 27.0–27.1 kg m^{-3} isopycnal range OMP results, we assumed that the PFZ water fractional content of the SAMW should have increased by approximately 0.15 for every 15° of longitude (Figure 10). The initial mixed layer temperature and salinity were therefore evolved downstream by mixing a 0.15 fraction of PFZ water into the mixed layer. This evolution was performed for two iterations, each of which incorporated a 0.15 fraction of PFZ water into the SAMW. This corresponded to an along-front movement of approximately 30°, at which point the mixed layer characteristics should have approximated the profiles observed in the cruise's eastern sections near 73°W. The PFZ water properties were defined by the first mixed layer immediately south of the SAF in each case (along 103°W for the first iteration and along 89°W for the second iteration).

[40] The bulk calculation suggests that cross-frontal exchange could cause the downstream evolution of SAMW mixed layer properties, as the evolution of the temperature and salinity properties of the mixed layers in the bulk calculation mirrors the along-front freshening and cooling of the SAMW mixed layers observed by Argo (Figure 12). The SAMW mixed layers in the bulk calculation freshened by 0.04 psu and cooled by 0.5°C due to cross-frontal exchange. The Argo-observed SAMW freshened by 0.08 psu and cooled by 1.0°C between 103°W and 77°W. These values were computed by averaging the properties of the SAMW MLDs deeper than 400 m in two bins: profiles from 100°W to 95°W and profiles from 75°W to 80°W. The slight discrepancy between our bulk calculation and the Argo observations could be due to increased cross-frontal exchange at the ocean surface not captured in our isopycnal averages, as well as the continual along-front cooling and freshening of the PFZ water being exchanged into the SAMW formation region that was not fully included in our simple calculation.

[41] These results suggest that cross-frontal exchange substantially contributes to the downstream evolution of SAMW properties, a result consistent with many recent studies. *Sallée et al.* [2006] found that Ekman transport of

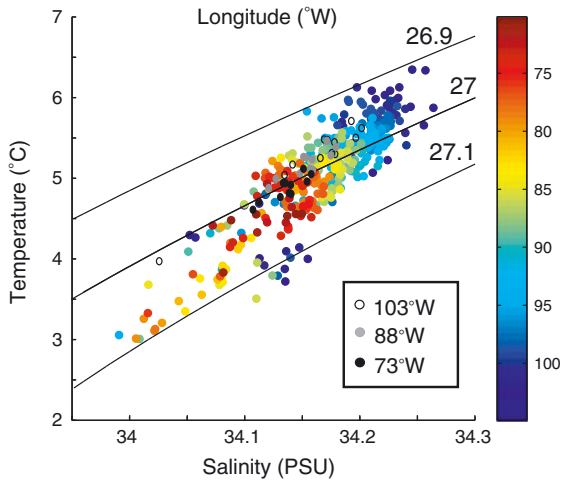

Figure 12. Mixed layer temperature-salinity diagram for Argo profiles collected in the cruise region with MLDs deeper than 300 m; the color corresponds to the profile longitude. Plotted over the Argo data are the results of a simple bulk calculation. The bulk calculation was initialized with mixed layers from the 2005 austral winter cruise section along 103°W (open circles). The mixed layers were evolved with bulk cross-frontal fluxes that increased the fractional content of PFZ water by 0.15. The PFZ water was represented by the mean of the first three mixed layers south of the SAF along 103°W. This mixed layer was further evolved by a second iteration of cross-frontal exchange that increased the PFZ water fractional content by an additional 0.15. For this iteration the PFZ water was represented by the mean of the first three mixed layers south of the SAF along 89°W. The evolved downstream mixed layers are plotted in grey (88°W) and black (73°W). Potential density (black lines) is contoured at 0.1 kg m^{-3} intervals from 26.9 to 27.1 kg m^{-3}. The Argo MLDs were calculated following [*Holte and Talley*, 2009].

cold and fresh water from the south was consistent with the loss of salt and heat in the SAMW mixed layers in the Indian Ocean. *Sallée et al.* [2008] found that wintertime Ekman heat advection and eddy heat diffusion in the mixed layer had a cooling influence on SAMW in the southeast Pacific. *Saenko et al.* [2003] identified the southeast Pacific as a region of strong freshwater export from the south, a result consistent with our study. Studies looking at the temporal variability of SAMW properties have long cited Ekman transport as a prime source of variability [*Rintoul and England*, 2002]. *Naveira-Garabato et al.* [2009] found that the Ekman transport of Antarctic surface waters from the south contributed significantly to SAMW freshening and cooling from 1990 to 2005. *Holte et al.* [2012] demonstrated that air-sea fluxes were necessary for forming the deep SAMW mixed layers, but did little to change their properties; cross-frontal exchange offers a viable mechanism for explaining the along-front evolution of SAMW properties in the southeast Pacific. Cross-frontal exchange also acts as a conditioning factor for the formation of deep SAMW mixed layers in winter, as it modifies the stratification and heat content in the SAMW formation region, making it easier for air-sea heat fluxes to drive deep mixing during winter. These findings provide an alternative theory to *McCartney* [1977], who proposed that the cumulative effects of heat loss and precipitation were the sole mechanisms for modifying SAMW along the ACC path.

[42] The "rate" of cross-frontal exchange diagnosed in our analysis applies only to the southeast Pacific, as the strength of the intrusions, Ekman transport, and eddies driving the exchange vary along the SAF. *Gille* [1999] noted that meridional exchange across the ACC was likely to vary substantially geographically. *Ansorge et al.* [2006] and *Sallée et al.* [2006] have shown that eddy shedding is strongly dependent on bottom bathymetry. *Shuckburgh et al.* [2009] found that eddy diffusivity in the ACC is suppressed by strong mean flow. An improved understanding of the mechanisms controlling SAMW's properties, including cross-frontal exchange, will help scientists to interpret observations of SAMW's temporal and spatial variability. Similarly, our result, as do the others, implies that to correctly model SAMW, the models must correctly capture cross-frontal exchange, a very complex problem as noted in *Treguier et al.* [2007].

[43] **Acknowledgments.** NSF Ocean Sciences grant OCE-0327544 supported L.D.T., T.K.C., and J.H. and funded the two research cruises; NSF Ocean Sciences grant OCE-0850869 funded part of the analysis. BMS's contribution to this work was undertaken as part of the Australian Climate Change Science Program, funded jointly by the Department of Climate Change and CSIRO. Thanks to the crew of the R/V Knorr and the Oceanographic Data Facility at SIO for helping us collect such a rich data set. The altimeter dynamic topography fields are produced by Ssalto/Duacs and distributed by AVISO with support from Centre National d'Etudes Spatiales. The comments of three reviewers greatly improved the manuscript.

References

Abernathey, R., J. Marshall, M. Mazloff, and E. Shuckburgh (2010), Enhancement of mesoscale eddy stirring at steering levels in the Southern Ocean, *J. Phys. Oceanogr.*, *40*, 170–184, doi:10.1175/2009JPO4201.1.

Ansorge, I. J., J. R. E. Lutjeharms, N. C. Swart, and J. V. Durgadoo (2006), Observational evidence for a cross frontal heat pump in the Southern Ocean, *Geophys. Res. Lett.*, *33*, L19601, doi:10.1029/2006GL026174.

Beal, L. M., T. K. Chereskin, Y. D. Lenn, and S. Elipot (2006), The sources and mixing characteristics of the Agulhas current, *J. Phys. Oceanogr.*, *36*, 2060–2074, doi:10.1175/JPO2964.1.

Bower, A. S., H. T. Rossby, and J. L. Lillibridge (1985), The Gulf Stream – Barrier or blender? *J. Phys. Oceanogr.*, *15*, 24–32.

Bower, A. S., and T. Rossby (1989), Evidence of cross-frontal exchange processes in the Gulf Stream based on isopycnal RAFOS float data, *J. Phys. Oceanogr.*, *19*, 1177–1190.

Budillon, G., M. Pacciaroni, S. Cozzi, P. Rivaro, G. Catalano, C. Ianni, and C. Cantoni (2003), An optimum multiparameter mixing analysis of the shelf waters in the Ross Sea, *Antarct. Sci.*, *15*, 105–118, doi:10.1017/S095410200300110X.

Chereskin, T. K., L. D. Talley, and B. M. Sloyan (2010), Nonlinear vorticity balance of the Subantarctic Front in the southeast Pacific, *J. Geophys. Res. Oceans*, *115*, 6026, doi:10.1029/2009JC005611.

Dong, S., J. Sprintall, S. T. Gille, and L. Talley (2008), Southern Ocean mixed-layer depth from Argo float profiles, *J. Geophys. Res. Oceans*, *113*, 6013, doi:10.1029/2006JC004051.

England, M. H., J. S. Godfrey, A. C. Hirst, and M. Tomczak (1993), The mechanism for Antarctic Intermediate Water renewal in a world ocean model, *J. Phys. Oceanogr.*, *23*, 1553–1560.

Ferrari, R., and M. Nikurashin (2010), Suppression of eddy diffusivity across jets in the Southern Ocean, *J. Phys. Oceanogr.*, *40*, 1501–1519, doi:10.1175/2010JPO4278.1.

Frants, M., S. Gille, C. Hewes, O. Holm-Hansen, M. Kahru, A. Lombrozo, C. Measures, B. G. Mitchell, H. Wang, and M. Zhou (2012), Optimal multiparameter analysis of source water distributions in the southern drake passage, *Deep Sea Res. II*, doi:10.1016/j.dsr2.2012.06.002.

Gille, S. T. (1999), Mass, heat, and salt transport in the southeastern Pacific: A circumpolar current inverse model., *J. Geophys. Res.*, *104*, 5191–5210, doi:10.1029/1998JC900106.

Hanawa, K., and L. D. Talley (2001), Mode waters, in *Ocean Circulation and Climate*, edited by Siedler, G., J. Church, and J. Gould, pp. 373–386, Academic Press, London.

Hartin, C. A., R. A. Fine, B. M. Sloyan, L. D. Talley, T. K. Chereskin, and J. Happell (2011), Formation rates of Subantarctic mode water and Antarctic intermediate water within the South Pacific, *Deep Sea Res. Part I: Oceanographic Research*, *58*, 524–534, doi: 10.1016/j.dsr.2011.02.010.

Herraiz-Borreguero, L., and S. R. Rintoul (2010), Subantarctic mode water variability influenced by mesoscale eddies south of Tasmania, *J. Geophys. Res. Oceans*, *115*, 4004, doi:10.1029/2008JC005146.

Hinrichsen, H., and M. Tomczak (1993), Optimum multiparameter analysis of the water mass structure in the western North Atlantic ocean, *J. Geophys. Res.*, *98*, 10155–10170.

Holte, J., and L. Talley (2009), A new algorithm for finding mixed layer depths with applications to Argo data and Subantarctic mode water formation, *J. Atmos. Oceanic Technol.*, *26*, 1920–1939, doi: 10.1175/2009JTECHO543.1.

Holte, J. W., L. D. Talley, T. K. Chereskin, and B. M. Sloyan (2012), The role of air-sea fluxes in Subantarctic mode water formation, *J. Geophys. Res. Oceans*, *117*, 3040, doi:10.1029/2011JC007798.

Ito, T., M. Woloszyn, and M. Mazloff (2010), Anthropogenic carbon dioxide transport in the Southern Ocean driven by Ekman flow, *Nature*, *463*, 80–83, doi:10.1038/nature08687.

Jayne, S. R., and J. Marotzke (2002), The oceanic eddy heat transport, *J. Phys. Oceanogr.*, *32*, 3328–3345, doi:10.1175/1520-0485(2002)032 <3328:TOEHT>2.0.CO;2.

Joyce, T. M. (1977), A note on the lateral mixing of water masses, *J. Phys. Oceanogr.*, *7*, 626–629.

Joyce, T. M., L. N. Thomas, and F. Bahr (2009), Wintertime observations of Subtropical mode water formation within the Gulf Stream, *Geophys. Res. Lett.*, *360*, 2607, doi:10.1029/2008GL035918.

Karsten, R., and J. Marshall (2002), Constructing the residual circulation of the ACC from observations, *J. Phys. Oceanogr.*, *32*, 3315–3327, doi: 10.1175/1520-0485(2002)032<3315:CTRCOT>2.0.CO;2.

Keeling, R. F., and B. B. Stephens (2001), Antarctic sea ice and the control of Pleistocene climate instability, *Paleoceanography*, *16*, 112–131.

Kerr, R., M. M. Mata, and C. A. E. Garcia (2009), On the temporal variability of the Weddell Sea Deep Water masses, *Antarct. Sci.*, *21*, 383–400, doi:10.1017/S0954102009001990.

Klein, B., and M. Tomczak (1994), Identification of diapycnal mixing through optimum multiparameter analysis. 2. Evidence for unidirectional diapycnal mixing in the front between North and South Atlantic Central Water, *J. Geophys. Res.*, *99*, 25275–25280.

Leffanue, H., and M. Tomczak (2004), Using OMP analysis to observe temporal variability in water mass distribution, *J. Mar. Syst.*, *48*, 3–14, doi: 10.1016/j.jmarsys.2003.07.004.

Lenn, Y.-D., and T. K. Chereskin (2009), Observations of Ekman currents in the Southern Ocean, *J. Phys. Oceanogr.*, *39*, 768–779, doi: 10.1175/2008JPO3943.1.

Marshall, J., E. Shuckburgh, H. Jones, and C. Hill (2006), Estimates and implications of surface eddy diffusivity in the Southern Ocean derived from tracer transport, *J. Phys. Oceanogr.*, *36*, 1806–1821, doi: 10.1175/JPO2949.1.

McCartney, M. S. (1977), Subantarctic mode water, in *A Voyage of Discovery: George Deacon 70th Anniversary Volume*, edited by M. V. Angel, pp. 103–119, Pergamon, Oxford.

McCartney, M. S. (1982), The subtropical recirculation of mode waters, *J. Mar. Res.*, *24*, 427–464

Morrow, R., J. Donguy, A. Chaigneau, and S. Rintoul (2004), Cold-core anomalies at the Subantarctic front, south of Tasmania, *Deep Sea Res., Part I*, *51*, 1417–1440, doi:10.1016/j.dsr.2004.07.005.

Naveira-Garabato, A. C., L. Jullion, D. P. Stevens, K. J. Heywood, and B. A. King (2009), Variability of Subantarctic mode water and Antarctic intermediate water in the drake passage during the late-twentieth and early-twenty-first centuries, *J. Climate*, *22*, 3661–3688, doi:10.1175/2009JCLI2621.1.

Orsi, A. H., T. Whitworth, and W. D. Nowlin (1995), On the meridional extent and fronts of the Antarctic circumpolar current, *Deep Sea Res. Part I: Oceanographic Research*, *42*, 641–673.

Owens, W. B. (1984), A synoptic and statistical description of the Gulf Stream and subtropical gyre using SOFAR floats, *J. Phys. Oceanogr.*, *14*, 104–113.

Pahnke, K., and R. Zahn (2005), Southern hemisphere water mass conversion linked with North Atlantic climate variability, *Science*, *307*, 1741–1746, doi:10.1126/science.1102163.

Park, Y., and L. Gambéroni (1997), Cross-frontal exchange of Antarctic intermediate water and Antarctic bottom water in the Crozet basin, *Deep Sea Res. Part II: Topical Studies in Oceanography*, *44*, 963–986.

Poole, R., and M. Tomczak (1999), Optimum multiparameter analysis of the water mass structure in the Atlantic Ocean thermocline, *Deep Sea Res. I*, *46*, 1895–1921.

Redfield, A., B. H. Ketchum, and F. A. Richards (1963), The influence of organisms on the composition of sea-water, in *The Sea: Ideas and Observations on Progress in the Study of the Seas*, edited by M. N. Hill, pp. 26–77, Springer-Verlag, Berlin Heidelberg, London.

Rintoul, S., and M. England (2002), Ekman transport dominates local air-sea fluxes in driving variability of Subantarctic mode water, *J. Phys. Oceanogr.*, *32*, 1380–1321, doi:10.1175/1520-0485(2002)032<1308: ETDLAS>2.0.CO;2.

Ruddick, B. (2003), Oceanic thermohaline intrusions: Observations, *Prog. Oceanogr.*, *56*, 499–527, doi:10.1016/S0079-6611(03)00028-4.

Saenko, O. A., A. J. Weaver, and M. H. England (2003), A region of enhanced northward Antarctic intermediate water transport in a coupled climate model, *J. Phys. Oceanogr.*, *33*, 1528–1535, doi:10.1175/1520-0485(2003)033<1528:AROENA>2.0.CO;2.

Sallée, J., K. Speer, S. Rintoul, and S. Wijffels (2010), Southern Ocean thermocline ventilation, *J. Phys. Oceanogr.*, *40*, 509–529, doi: 10.1175/2009JPO4291.1.

Sallée, J.-B., R. Morrow, and K. Speer (2008), Eddy heat diffusion and Subantarctic mode water formation., *Geophys. Res. Lett.*, *350*, 5607, doi: 10.1029/2007GL032827.

Sallée, J.-B., N. Wienders, K. Speer, and R. Morrow (2006), Formation of Subantarctic mode water in the southeastern Indian Ocean, *Ocean Dyn.*, *56*, 525–542, doi:10.1007/s10236-005-0054-x.

Shuckburgh, E., H. Jones, J. Marshall, and C. Hill (2009), Understanding the regional variability of eddy diffusivity in the Pacific sector of the Southern Ocean, *J. Phys. Oceanogr.*, *39*, 2011–2023, doi: 10.1175/2009JPO4115.1.

Sloyan, B., and S. Rintoul (2001), Circulation, renewal, and modification of Antarctic mode and intermediate water, *J. Phys. Oceanogr.*, *31*, 1005–1030.

Sloyan, B., L. Talley, T. Chereskin, R. Fine, and J. Holte (2010), Antarctic intermediate water and Subantarctic mode water formation in the southeast Pacific: The role of turbulent mixing, *J. Phys. Oceanogr.*, *40*, 1558–1574, doi:10.1175/2010JPO4114.1.

Smith, K. S., and J. Marshall (2009), Evidence for enhanced eddy mixing at middepth in the Southern Ocean, *J. Phys. Oceanogr.*, *39*, 50–69, doi: 10.1175/2008JPO3880.1.

Sokolov, S., and S. R. Rintoul (2009a), Circumpolar structure and distribution of the Antarctic circumpolar current fronts: 1. Mean circumpolar paths, *J. Geophys. Res. Oceans*, *114*, 11018, doi:10.1029/ 2008JC005108.

Sokolov, S., and S. R. Rintoul (2009b), Circumpolar structure and distribution of the Antarctic circumpolar current fronts: 2. Variability and relationship to sea surface height, *J. Geophys. Res. Oceans*, *114*, 11019, doi:10.1029/2008JC005248.

Speer, K., S. Rintoul, and B. Sloyan (2000), The diabatic deacon cell, *J. Phys. Oceanogr.*, *30*, 3212–3222.

Talley, L. D. (1996), Antarctic intermediate water in the South Atlantic, in *The South Atlantic: Present and Past Circulation*, edited by G. Wefer, W. Berger, G. Siedler, and D. Webb, pp. 219–238, Springer-Verlag, Berlin Heidelberg, Germany.

Tomczak, M., and D. G. B. Large (1989), Optimum multiparameter analysis of mixing in the thermocline of the Eastern Indian Ocean, *J. Geophys. Res.*, *94*, 16141–16149.

Treguier, A. M., M. H. England, S. R. Rintoul, G. Madec, J. Le Sommer, and J.-M. Molines (2007), Southern Ocean overturning across streamlines in an eddying simulation of the Antarctic circumpolar current, *Ocean Sci.*, *3*, 491–507, doi:10.5194/os-3-491-2007.

Vivier, F., D. Iudicone, F. Busdraghi, and Y.-H. Park (2010), Dynamics of sea-surface temperature anomalies in the Southern Ocean diagnosed from a 2D mixed-layer model, *Clim. Dyn.*, *34*, 153–184, doi:10.1007/s00382-009-0724-3.

Wang, X., and R. J. Matear (2001), Modeling the upper ocean dynamics in the Subantarctic and polar frontal zones in the Australian sector of the Southern Ocean, *J. Geophys. Res.*, *106*, 31511–31524.